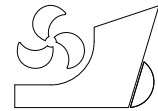


Smiljko Rudan
Luka Drobilo



ISSN 0007-215X
eISSN 1845-5859

NFEM ANALYSIS OF A COMPOSITE MADE HULL OF AUTONOMOUS UNDERWATER SUBMERSIBLE

UDC 629.58
Professional paper

Summary

Due to their specific properties composite materials are being used in a variety of structures. Modern underwater vehicles are a good example: they are light, sturdy and corrosion resistant. Demands posed on such a structures are good sailing properties, good maneuverability and the ability to withstand designed pressure. Nonlinear finite element method (NFEM) is a sophisticated engineering tool that may be used to estimate limitations in the composite-made submersible design. However, the application of the method is not always straightforward. Commercially available NFEM software provides a number of material models but their application is limited by the available material properties. In addition, numerical problems may occur and both material model and numerical model must be verified against instabilities. A particular submersible is being modeled and subjected to NFEM analysis. The overview of commercial software material models is given and their application in structural analysis of a submersible is evaluated. Comparison is made between different structural materials in order to check the submersible maximum diving depth. Numerical problems are commented, different material solutions compared and structure enhancements proposed.

Key words: *glass fibre; carbon fibre; finite element analysis (FEA); autonomous underwater vehicles (AUV)*

1. Introduction

Remotely Operated Vehicles (ROV) are used extensively in various scientific, industrial and military applications due to significant reduction of costs and risks in comparison with human operated devices. However, they need to be controlled via physical power and information link which increases logistic efforts and limits their operability. By the advance of technology a generation of modern Autonomous Underwater Vehicles (AUV) is being designed. They are equipped with their own power supply and operated by wireless connection. As long as they have power, they are able to operate. A design of such a device is, however, a complex task.

One particular design of an AUV submersible was proposed and analysed within the University of Zagreb on an interdisciplinary project that joined Faculty of Mechanical Engineering and Naval Architecture and Faculty of Electrical Engineering and Computing, Fig. 1. Both students and researchers were involved in the design of a small submersible with a prospect to have a good manoeuvrability, high autonomy and adequate sailing properties. In particular, maximum diving depth of a submersible is set to be 150 m, resulting in a load pressure of 15 bars. This condition itself poses a significant demand on the structure and is considered in detail within this work.

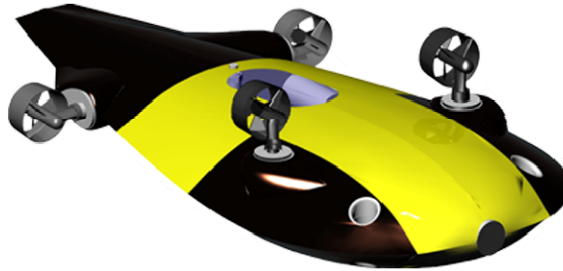


Fig. 1 Rendered view of the submersible prototype

The submersible hull has a hydrodynamic shape and holds the attached propulsion motors. In order to comply with the deep dive request, the submersible structure is divided in two parts. The “dry” part contains all of the electronic equipment, i.e. sensors, cameras, engines and batteries. This part of the submersible is sealed and subjected to surrounding water pressure. The “wet” part of submersible is attached to the dry section and is flooded when submerged in the surrounding fluid (water). Since the wet part is not affected by hydrostatic pressure it is made of a common polymer material (plastic) and it will not be of further concern in this article.

The choice of the dry section material is crucial. The material must provide adequate strength, which then determines the ultimate capacity of the structure and maximum diving depth of the submersible. At the same time, the resistance to deformation is equally important. In its original shape the submersible has slightly positive buoyancy. Excessive deformation may alter the dry section volume and reduce the submersible buoyancy. Should the equilibrium between weight and buoyancy be altered so that weight dominates, uncontrolled sinking of the submersible may occur.

Composite materials, in particular glass or carbon reinforced plastics, may have properties that suit the purpose of constructing a capable submersible. They are tailored by assembling matrix and reinforcement constituents into a composite material which results in unique physical and mechanical properties. Such materials are easily shaped, lightweight and corrosion proof. Three composite materials will be considered:

- Material 1: in-house made glass-fiber/epoxy,
- Material 2: higher strength glass-fiber/epoxy [1] and
- Material 3: carbon-fiber/epoxy [2].

Furthermore, three variations of the material 1 are produced, denominated as materials 1A, 1B and 1C, so that the strongest one can be recognized. A three-point bending test is performed for that purpose.

Structural analyses are performed in the commercial nonlinear FEM code, namely LS-DYNA. Four different LS-DYNA material models were considered: MAT22, MAT54, MAT55 and MAT59 so that most suitable one can be recognized. Numerical simulation of the

three-point bending test is performed for that purpose. A short overview of the corresponding failure criteria for each material model will be given.

Finally, structural analysis of the submersible dry hull is performed for materials 1B, 2 and 3, described through the LS-DYNA material model 54. Fig. 2 illustrates the procedure.

It should be noted that the application of highly sophisticated software for the analysis of relatively simple structure may seem to be not justified. However, since the same software is regularly used on much more complex structures and analysis, the aim of the paper is to demonstrate the process of performing such analysis on a less complicated example, as well as to show some of the issues that can arise even on such a relatively simple problem.

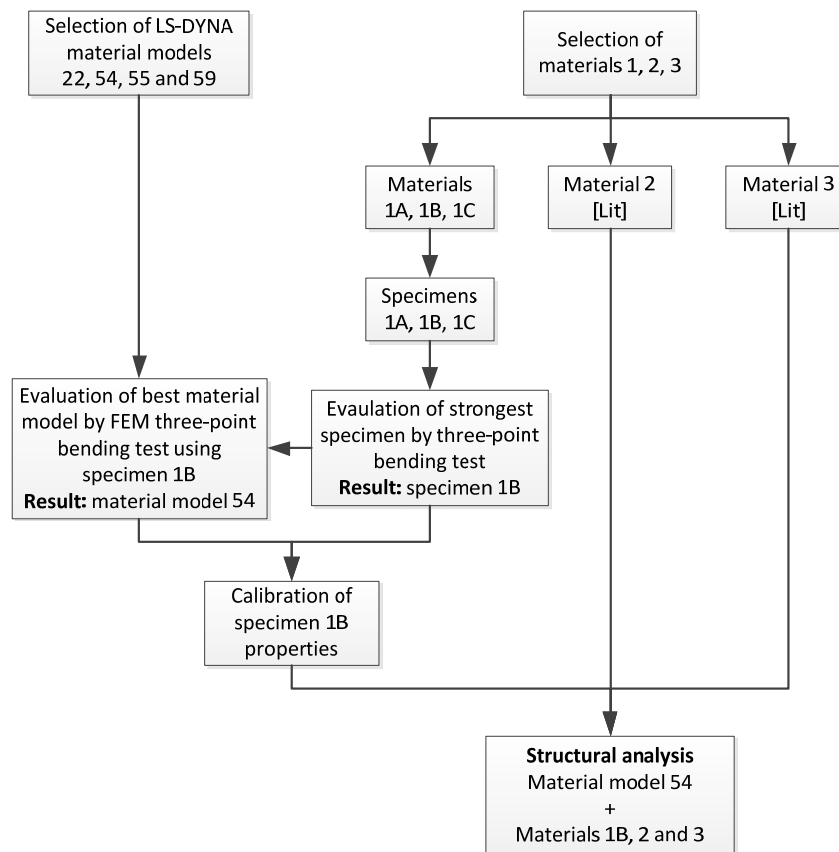


Fig. 2 Evaluation procedure overview

2. Hull material considerations

Dry hull prototype is built using in-house made glass-fiber epoxy composite i.e. material 1. Since the dry hull shape is relatively complex it is not obvious which stress components will be of prevailing importance when the hydrostatic load is applied. Due to that, it is impossible to anticipate the most efficient fiber orientation. Therefore, three variants of material 1 are produced and denominated as materials 1A, 1B and 1C respectively. Each material constitutes of two “MAT” fiber layers and two “ROVING” fiber layers [3]. “MAT” fiber has random fiber orientation while “ROVING” fiber in this case has two distinguished fiber directions intersecting at a 90 degree angle. Materials 1A, 1B and 1C internal structure, with "ROVING" fiber intersection at 45, 0 and 90 degrees, respectively, is presented in Fig. 3. It should be noted that composite materials 1A, 1B and 1C are constructed so to have nearly equal strength in both longitudinal and transversal direction.

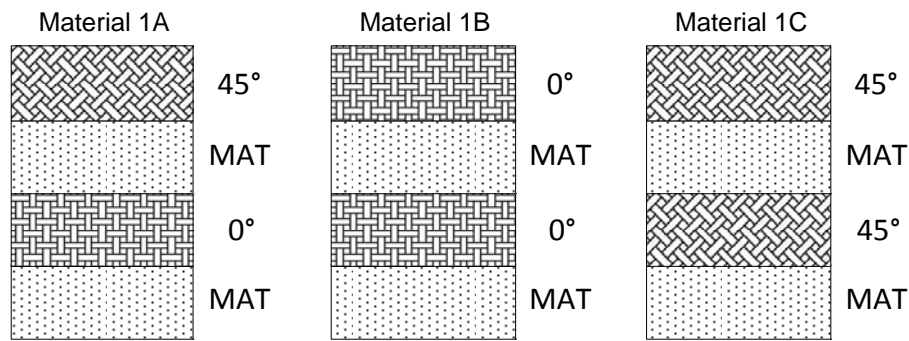


Fig. 3 ROVING and MAT layers in Material 1A, 1B and 1C specimens

Since hydrostatic pressure is acting on the dry hull, it is expected that bending will be the prevailing deformation. Therefore, specimens made of materials 1A, 1B and 1C were subjected to three-point-bending test in order to evaluate their bending strength. The test is being performed at the Faculty of Mechanical Engineering and Naval Architecture Laboratory for non-metal materials. Universal testing machine ZMG VEB Thuringer 4800N was used to perform the tests according to HRN EN ISO 14125 norm. Specimens, having a size of 42x21x2 mm (length x width x thickness), were then supported at the ends and subjected to load via cylindrical intender. Load was increased in steps of 10N until rupture. Five specimens of each material were tested and material 1B was found to have the highest bending strength. Due to that, materials 1A and 1C were not of further concern. The resulting force-displacement curves for five specimens of material 1B, including their mean, are presented in Fig. 4. Results for the specimen 1 differ significantly and are discarded. It should be noted that, due to the orientation of the fiber, three-point-bending test may put material 1B "in favor". The matter was not further studied here but caution is needed in judging the material properties when different fiber orientation is used.

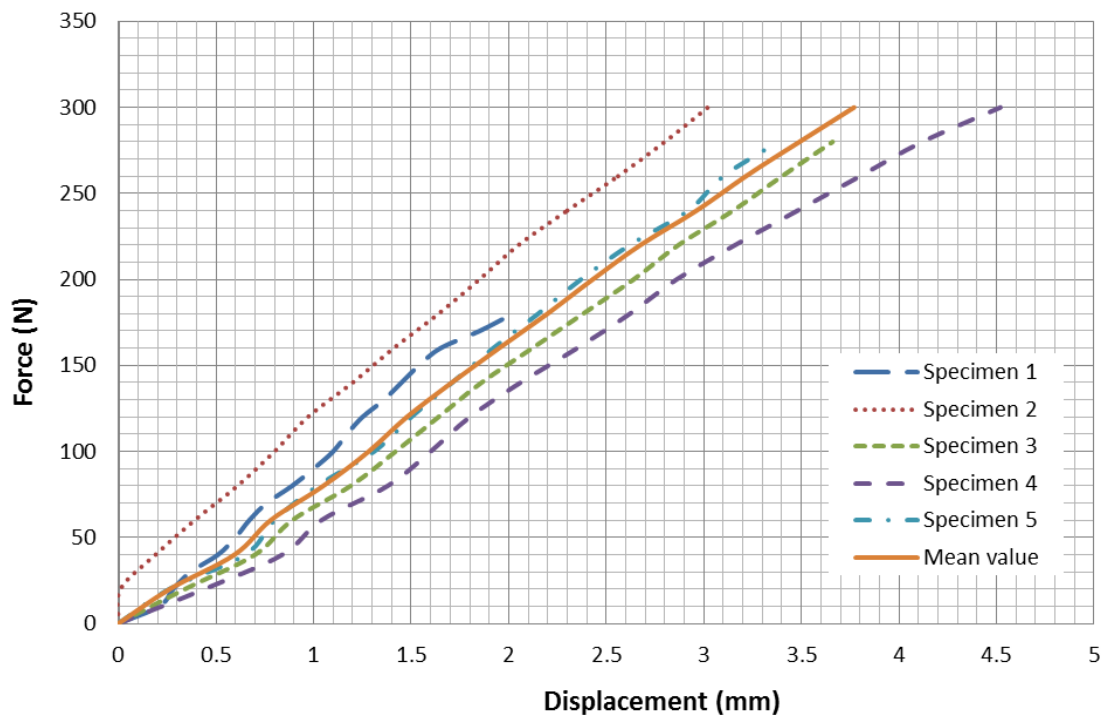


Fig. 4 Three-point bending test results of material 1B specimens

3. Material models

LS-DYNA is commercially available software capable of, among other, explicit nonlinear finite element analysis. It provides a number of different material models i.e. numerical formulations of different material properties. Choice of a proper material model is essential since results directly depend on it. In addition, since composite materials constitute from two or more materials, special care is needed. Composite materials, according to LSTC recommendation [4], may be analysed by several material models of which the following four are selected here: MAT22 – composite_damage, MAT54 and MAT55 – enhanced_composite_damage, and MAT59 – composite_failure_shell_model. Other available material models were not considered due to various reasons, mostly because of unavailability of requested material properties. Other than MAT59, which is to be used for fabric material modelling, the mentioned material models are formulated for modelling unidirectional composite materials. However, due to the simplicity of their formulation and provision of adequate failure criteria they are successfully applied in the analysis of complex structures, such as e.g. (Heimbs 2009 [5], Kang et. al 2012 [6], Liu et. al 2013 [7]). The following failure criteria for the selected material models are based on the formulations stated in [8].

3.1 MAT22 – composite_damage

For defining the failure criteria in the material model 22, the Chang-Chang Composite Failure Model is used. Five material parameters are used in the three failure criteria. These are:

- S_1 – longitudinal tensile strength
- S_2 – transverse tensile strength
- S_{12} – shear strength
- C_2 – transverse compressive strength
- α – nonlinear shear stress parameter

S_1, S_2, S_{12} and C_2 are obtained from material strength measurement, α is defined by material shear stress-strain measurements. Failure is assumed whenever the value of at least one of the failure criteria is greater than 1. The three failure criteria are: matrix cracking, compression failure, fiber breakage and are defined as follows:

$$F_{matrix} = \left(\frac{\sigma_2}{S_2} \right)^2 + \bar{\tau} \quad (1)$$

$$F_{comp} = \left(\frac{\sigma_2}{2S_{12}} \right)^2 + \left[\left(\frac{C_2}{2S_{12}} \right)^2 - 1 \right] \frac{\sigma_2}{C_2} + \bar{\tau} \quad (2)$$

$$F_{fiber} = \left(\frac{\sigma_1}{S_1} \right)^2 + \bar{\tau} \quad (3)$$

3.2 MAT54 i MAT55 – enhanced_composite_damage

These models are very close in their formulations. Material model 54 uses the Chang matrix failure criterion (as does material model 22), and material model 55 uses the Tsay-Wu criterion for matrix failure. These material models enable various types of failure to be

specified, as well as special measures for failure under compression. A very detailed analysis of the capabilities and limitations of MAT54 is given in (Frankoboli 2012 [9]).

The Chang-Chang criteria is given as follows:

for the tensile fiber mode,

$$\sigma_{aa} > 0 \text{ then } e_f^2 = \left(\frac{\sigma_{aa}}{X_t} \right)^2 + \beta \left(\frac{\sigma_{ab}}{S_c} \right)^2 - 1 \begin{cases} \geq 0 \text{ failed} \\ < 0 \text{ elastic} \end{cases} \quad (4)$$

for the compressive fiber mode,

$$\sigma_{aa} < 0 \text{ then } e_c^2 = \left(\frac{\sigma_{aa}}{X_c} \right)^2 - 1 \begin{cases} \geq 0 \text{ failed} \\ < 0 \text{ elastic} \end{cases} \quad (5)$$

for the tensile matrix mode,

$$\sigma_{bb} > 0 \text{ then } e_m^2 = \left(\frac{\sigma_{bb}}{Y_t} \right)^2 + \left(\frac{\sigma_{ab}}{S_c} \right)^2 - 1 \begin{cases} \geq 0 \text{ failed} \\ < 0 \text{ elastic} \end{cases} \quad (6)$$

and for the compressive matrix mode,

$$\sigma_{bb} < 0 \text{ then } e_d^2 = \left(\frac{\sigma_{bb}}{2S_c} \right)^2 + \left[\left(\frac{Y_c}{2S_c} \right)^2 - 1 \right] \frac{\sigma_{bb}}{Y_c} + \left(\frac{\sigma_{ab}}{S_c} \right)^2 - 1 \begin{cases} \geq 0 \text{ failed} \\ < 0 \text{ elastic} \end{cases} \quad (7)$$

In the Tsay-Wu criteria the tensile and compressive fiber models are treated as in the Chang-Chang criteria. The failure criterion for the tensile and compressive matrix mode is given as:

$$e_{md}^2 = \frac{\sigma_{bb}^2}{Y_c Y_t} + \left(\frac{\sigma_{ab}}{S_c} \right)^2 + \frac{(Y_c - Y_t) \sigma_{bb}}{Y_c Y_t} - 1 \begin{cases} \geq 0 \text{ failed} \\ < 0 \text{ elastic} \end{cases} \quad (8)$$

3.3 MAT59 – composite_failure_shell_model

For the material model 59 detailed information is difficult to find. The material model is mentioned in the LSTC LS-DYNA Keyword User's Manual [10] where the necessary parameters are explained, but there is no mention of the failure criteria or any other information regarding the material model formulation. A short explanation of two different formulations of the material model (59a i 59b) are mentioned in [11]. In both cases the failure functions are defined by the material strength characteristics, while the material model 59a also enables an additional parameter to be set which further defines the tensile failure limitations.

4. NFEM simulation of three-point-bending test

A nonlinear finite element method simulations of the laboratory tests were performed to check the adequacy of LS-DYNA material models. Generic finite element model of the specimen was generated using 42x20 finite elements, each having a rectangular are of 1 mm², Fig. 5. The model is supported near the far edges of the specimen, i.e. at the location of support rollers in the laboratory test, as noted by the yellow lines in Fig. 5. The stress roller was modeled as a simple rigid cylinder moving in negative z-axis direction until the rupture of the specimen. Boundary conditions concerning the symmetry of the model were applied as well. Four different FE models were created, being the same except for material model formulation.

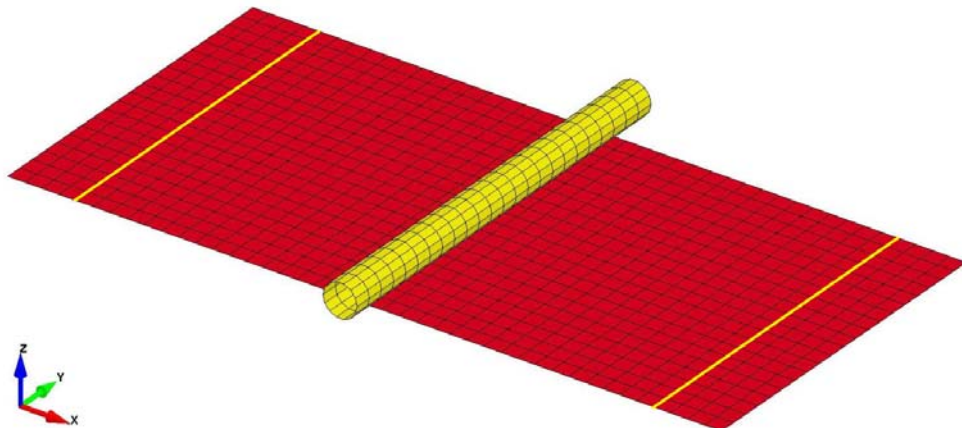


Fig. 5 FE model of a three-point bending test

Since composite material performance depends on the setup of their constituents (number of layers, fiber orientation etc.) it is difficult to determine its properties except by complex testing of the particular sample. Therefore, properties of the material 2 as given in [1] were used as starting-point properties except for the value of maximum matrix deformation before the failure which is taken from [12]. These starting-point parameters are introduced in each of the four FE models. NFEM analyses are performed and material parameters are iteratively altered until the numerical results coincided with laboratory test results. Since force-displacement curve is actually a straight line, the most influential parameter to be adjusted is longitudinal (x-axis) modulus of elasticity. Transversal (y-axis) modulus of elasticity and shear modulus was adjusted as well. The same procedure was followed for each material model. Since results differed significantly for the material models 22, 54 and 55 further adjustments were done: maximum fiber elongation was increased for material 54 and both compressive and shear stresses were reduced for material models 22 and 55. The outcome from these calibrations is presented by force-displacement curves in Fig. 6. Due to unrealistic behavior, material model 59 was excluded from further analysis. The limit force for all three remaining material models is now close to 300 N.

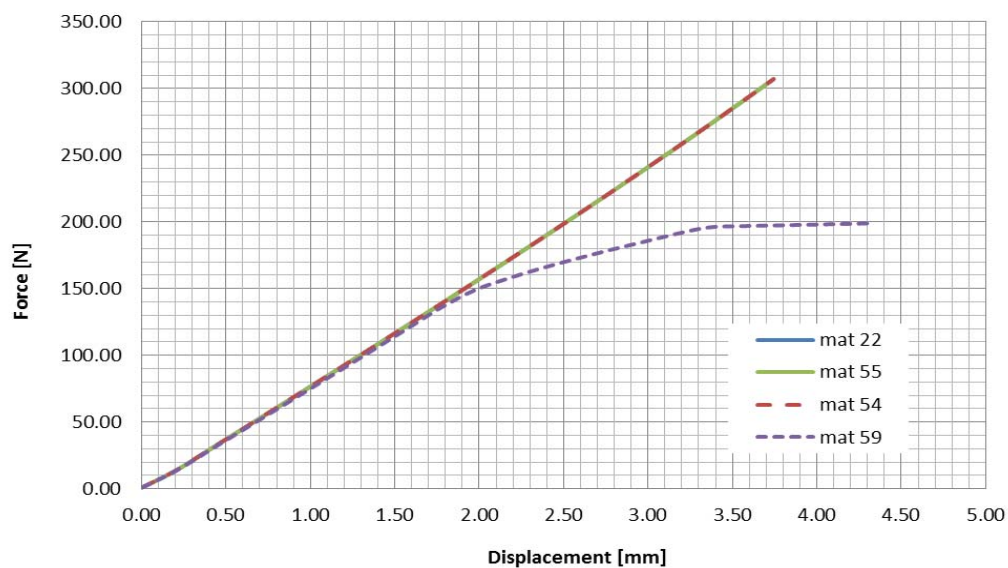


Fig. 6 Comparison of material models – FEM simulation of 3-point bending test

Since three material models enable accurate analysis, a comparative analysis of their properties was made. When material model 22 is in concern, the failure criteria may be modified either via material strength properties or through nonlinear shear stress parameter α . Material model 55 uses only material strength as the failure criteria. Material model 54 allows not only stress to be used as a failure criteria, but highest deformation of the composite material can also be defined, both for fiber compression and tension, shear and matrix. Due to this, material model 54 was selected as reference material model for the subsequent analysis of the submersible model. Calibrated material 1B properties are listed in Table 1. Fig. 7 presents comparison between experimental and numerical results using material model 54 in three-point-bending test NFEM simulation for Material 1B.

Table 1 Material properties

Property	Units	Material 1B in-house made glass/epoxy composite	Material 2 [1] glass/epoxy composite	Material 3 [2] carbon/epoxy composite
Density	[g/cm ³]	2,0	2,0	1,6
Poisson ratio	-	0,144	0,144	0,07
Young modulus longitudinal	[MPa]	4750	26600	70000
Young modulus transverse	[MPa]	4750	26600	70000
Shear modulus	[MPa]	3000	4630	6500
Longitudinal tensile strenght	[MPa]	170	422	963
Transverse tensile strenght	[MPa]	170	422	963
Longitudinal compressive strenght	[MPa]	170	410	873
Transverse tensile strenght	[MPa]	170	410	873
Shear strenght	[MPa]	50	121	99
Maximum fiber tension strain	[%]	3,6	1,85	1,25
Maximum fiber compression strain	[%]	3,6	2,0	1,5
Maximum matrix strain	[%]	8,5	8,5	8,58
Maximum shear strain	[%]	8,48	8,48	3,0

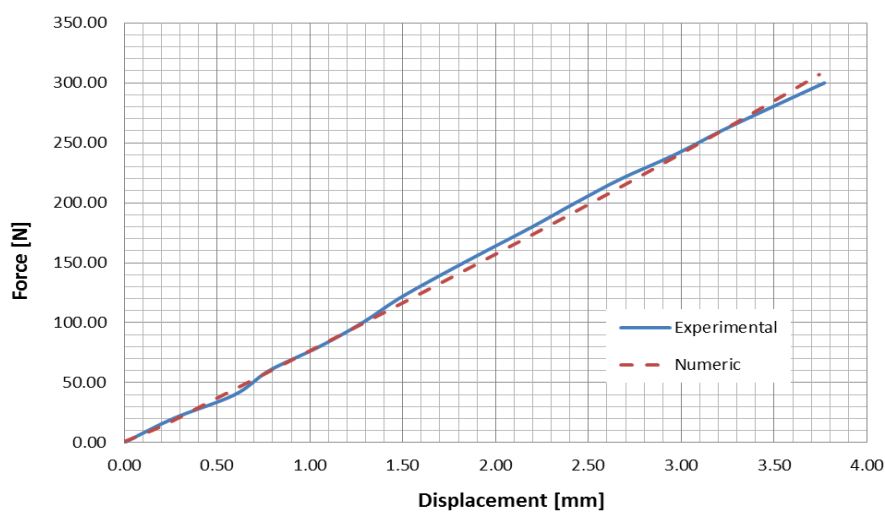


Fig. 7 Comparison of experimental and calibrated NFEM results for MAT54 and material 1B

5. Submersible structure

The submersible in concern was designed for operations such as sea bottom mapping, inspection of underwater sections of ship hulls and pipelines, search for lost or dangerous items, survey of archeological sites etc. Therefore, it should be able to sail safely in the Adriatic Sea currents, have at least 8 hours of autonomy, be as light as possible and easy to maintain. In addition: it needs to have six degree-of-freedom maneuverability and dynamic positioning system. Details on the preliminary submersible design and equipment are described in [13]. The propulsion system is the most significant single factor in design of such a submersible. Approximately 60% of the actual submersible mass and 65% of its volume are occupied by the elements of the propulsion system. This is directly related with the size and the resulting speed of the vessel. By using the CFD calculations main frame cross section was optimized and the submersible hull designed with minimum overall hydrodynamic resistance, Fig. 8. Resulting dimensions of the submersible are: length 1.05m, width 0.5m, height 0.21m and total volume 27.9 liters.

It should be noted that real-life manufacturing is subject to imperfections and errors (especially when working with the composite materials) so that the final product is unlikely to be equal to the theoretical model. Since the stiffness of the hull greatly relies on its form, depending on the range of deviations from the theoretical model, these imperfections embedded in the real-life structure could have certain impact on its durability and strength with regard to the numerical results.

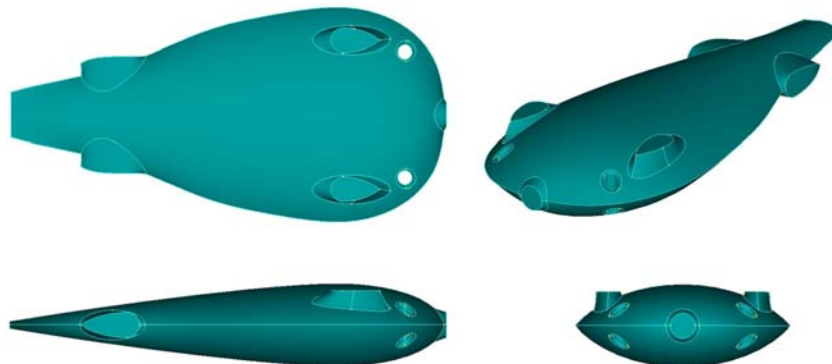


Fig. 8 Submersible model used for CFD calculations

6. Finite element model

Submersible finite element model was generated on the basis of the existing CAD model, Fig. 9. The model is divided into two parts, fore and aft part, which are connected at the main frame by screws. The camera and other glass windows may be noticed in front, on top and at the bottom of the submersible. Although CAD model separates the main frame in two, it is modeled as a single surface in the finite element model.

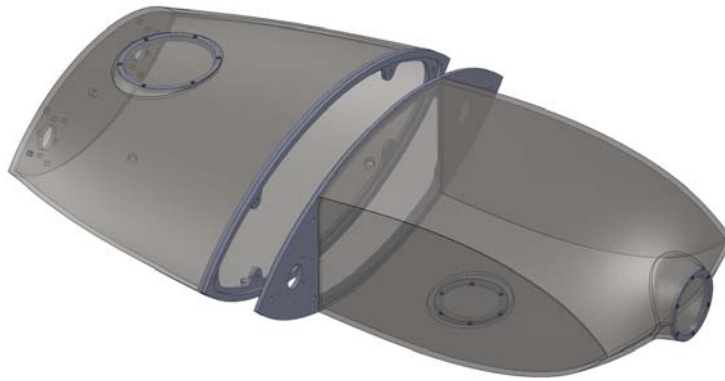


Fig. 9 Dry hull CAD model

Belytschko-Lin-Tsay 4-node shell finite elements were used to mesh the model geometry and the resulting FE model is presented in Fig. 10. Since glass-made windows are much stiffer than the composite-made structure, they are considered rigid in the FE model. The rest of the structure is modeled with finite elements having the thickness of 5 mm for the hull and 15 mm for the main frame.



Fig. 10 Dry hull FE model

The load consists of hydrostatic pressure only. During the analysis the pressure was increased from 0 to 15 bars, simulating submersible dive to 150 meters below surface. Boundary conditions were set on certain model nodes, indicated by the yellow dots in Fig. 10, in the following manner:

- Six main frame nodes at the circular openings: fixed x-translation (sub. length axis).
- Three nodes on upper glass-window: fixed z-translation (submersible width axis).
- Four edge nodes: fixed y-translation (submersible height axis).

In this way, the influence of boundary conditions is considered to be minimal, while assuring the realistic deformation of the model.

Three different materials were considered in the corresponding FE models, as described previously. Structural analysis was performed for each model and the summary of the results is listed in Table 2.

Table 2 Summary of MAT54 structural analysis results

Parametar	Material 1B	Material 2	Material 3
Submersible mass	9,51 kg	9,51 kg	8,2 kg
Number of finite elements	26294		
Number of nodes	26447		
Solver precision	Single precision		
Load increment	5 Pa / 1 s	50 Pa / 1 s	50 Pa / 1 s
Load duration	0,31 s	0,012 s	0,023 s
Computation time	7h 43min	42min	2h 7min
Achieved depth	15,5 m	60 m	115 m

Each model has equal number of nodes and finite elements, but due to differences in material properties they have a different mass. As expected, carbon-fiber/epoxy hull is lighter than glass-fiber/epoxy hull and the difference in mass is approximately 16%. Each analysis had an optimized set of control parameters so the analysis time differs. During the analysis single precision solver was used and dynamic effects were not allowed. It is clear that in-house made composite (material 1B) is the weakest material and as such allows the submersible to dive only up to 15.5 meters. By using the higher strength composite (material 2), diving depth increases to 60m. As expected, carbon-fiber/epoxy composite (material 3) is the strongest one and allows the submersible to dive up to 115m. The critical part of the hull is its main frame in each case.

In the case of material 1B, highest compressive stress was noticed in the main frame internal edge elements and prior to rupture its value is 168 MPa. Once the critical detail fails, Fig. 12, collapse of the structure occurs quickly in the following manner. Since material 1 is quite elastic the hull deforms more and more. Large, unsupported hull area is particularly affected. There are no structural elements that might stiffen the hull at this location so the structure relies only on material properties and geometry stiffness arising from the hull curvature. As ruptures spreads collapse becomes imminent and occurs in short time Fig. 11 (top).

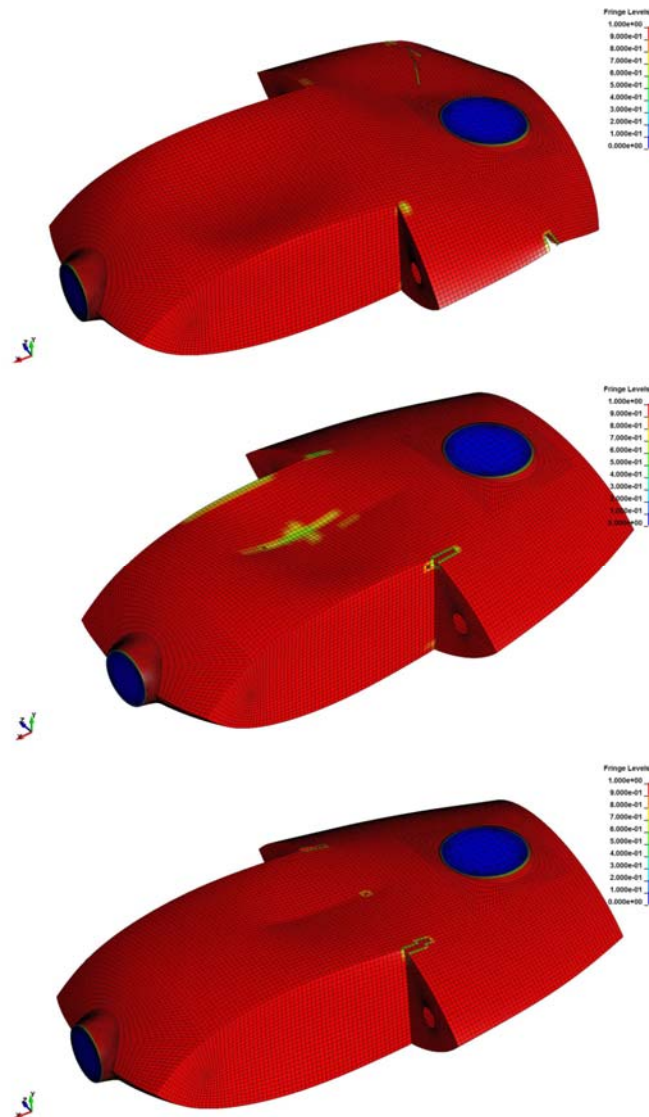


Fig. 11 Global failure - Mat 1 (top) Mat 2 (middle) Mat 3 (bottom)

In the case of material 2 the submersible hull can hold the hydrostatic pressure equivalent to 60 m water depth prior to first finite element failure. Soon after that several high stress locations are noticed over the hull area and after the first ruptures collapse follows quickly. Since the hull deformation is now less prominent, ruptures may be noticed also on the upper hull surface and close to rigid windows, Fig. 11 (middle).

In the case of material 3, the submersible hull can withstand hydrostatic pressure equivalent to 115 m water depth which is still below the design hydrostatic pressure. Due to increased stiffness hull deformations are smallest but cracks spread fast, Fig. 11 (bottom). The collapse mechanism in each case was not studied in detail, since it happens almost suddenly once the first element fails and is generally outside of the scope of this article.

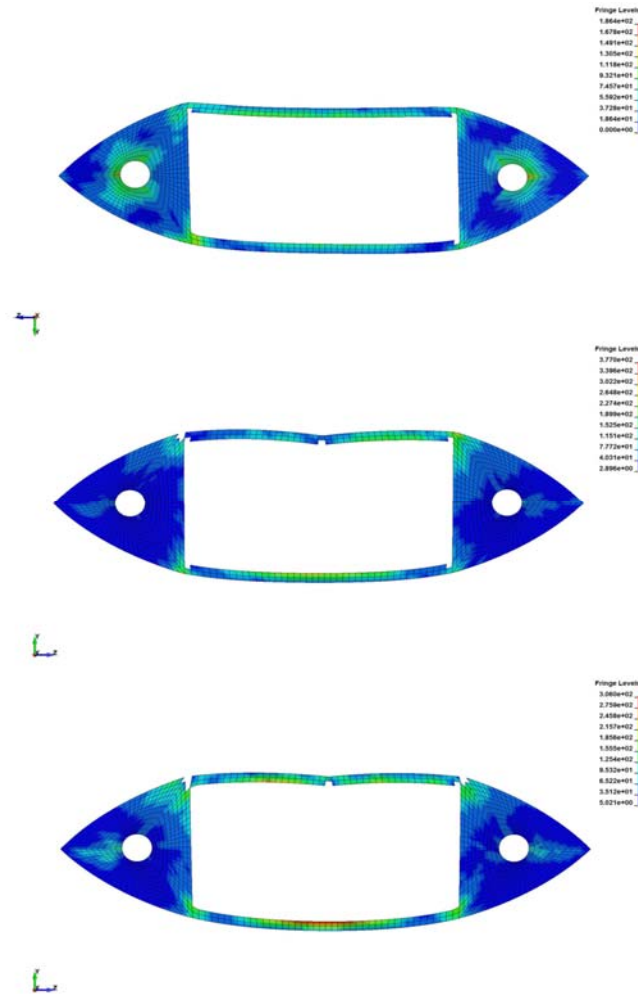


Fig. 12 Main rib failure - Mat 1 (top) Mat 2 (middle) Mat 3 (bottom)

7. Discussion of results

Structural analysis revealed critical structural details on the submersible dry hull. Stress concentration and initial ruptures occurred at nearly the same locations regardless of the material used. Since hull cross-section is ellipsoidal it has good initial stiffness and therefore provides resistance to overall deformation of the structure. However, as the load is increasing deformation of the hull becomes significant and finally its stiffness is lost. At that moment, hull main frame overtakes significant stress and becomes the critical component. The main frame arch is bending more and more as load is added. Due to that, corners of the arch become subjected to compressive stress concentration. Finally, the mostly stressed element fails and collapse is imminent. This scenario holds for all three materials. The problem of stress concentration was not further considered within this comparative analysis. Other than this, several possibilities exist to improve the main frame structure.

First, corners of the main frame arch may be shaped with bigger curvature radius. This itself will reduce the stress concentration and enable the surrounding structure to participate in stress redistribution. Second, the arches may be designed to be wider, Fig. 13 (right). This would add to structural resistance to deformation but may limit the cargo space. Third, main frame may be thicker, as much as technology allows. This would not add significantly to the overall mass of the structure and would reduce the main frame stress.

The problems of large, unsupported hull surfaces become obvious through the analysis. The presence of rigid glass-windows stiffens certain areas but large hull areas are completely un-stiffened. Even a small additional stiffness, e.g. by adding material to form some type of stiffener, would improve resistance of the hull to deformation. This solution must be evaluated carefully so that cargo space functionality is not obstructed.

Finally, longitudinal hull edges, connecting upper and lower part, have potential to initiate ruptures. Hull connections form rather sharp angle and since this area is obviously not used as cargo space additional material may be added. This probably holds for all the edges so certain amount of reinforcement of the structure may be gained this way. In addition, shell element modeling of connection edges represents worst-case scenario and detailed solid elements modeling is required if correct amount of material needs to be modeled. The same reasoning may hold for glass-made windows edges where more material exists in real structure than in the shell elements model.

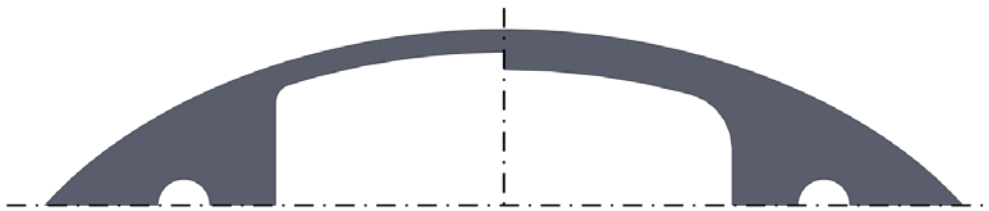


Fig. 13 Main frame structure – original (left) and improved (right)

Of the three materials concerned, carbon-fiber/epoxy material (material 3) proved to be strongest. However, if the same strength materials are used, a question of optimum elasticity modulus arises. Very stiff material will lead to high stress before sudden rupture, while very elastic material would lead to high deformation and consequent stress redistribution before rupture. Therefore, there exists an optimal value of modulus of elasticity. Since composites are assembled by choice and specific to the purpose, further research might enlighten this problem in detail.

Beside the effect of the elasticity modulus on the stiffness of the structure, its effect on the overall buoyancy needs to be taken in consideration as well. If the volume of the submersible dry hull is measured at the moment of rupture and compared to the initial volume, volume change for each material can be calculated. For material 1 a rather large decrease of 25.58% is measured, while the materials 2 and 3 show a 6.55% and 4.2% decrease of volume, respectively. This may have significant influence on the submersible behavior and should be taken into account.

8. Conclusion

A design of a small, composite-made submersible hull is evaluated through nonlinear FEM structural analysis. Three different construction materials are considered, namely: in house made glass-fibre/epoxy composite, higher strength glass-fiber/epoxy and carbon-fiber/epoxy. Most adequate fiber layout was determined by three-bending test of different specimens. Then, a numerical simulation of the three-point bending test is performed with a purpose of calibration of the material models. MAT54 was selected as optimal, general-purpose material model. Finally, structural analysis of the FEM hull models is performed using selected material model and all the three construction materials.

The task of the authors was to perform a nonlinear FEM analysis of the given autonomous underwater vehicle design and examine whether it can fulfill the project requirements. The goal of this article is to present the process of performing such analysis, including all the steps required in the process. A described procedure may be used during the

vessel design phase, when changes may be implemented, if necessary. Since a design of the particular submersible was done by a different group, which was in charge of performing the subsequent structural changes of it, the authors confined their present work to the task of obtaining the analysis results. However, after examining the results the authors have nevertheless showed some details they found to be critical weak spots and recommended several changes that should improve the design.

Structural analysis revealed the critical structural details, hull collapse mechanism and comparative advantages of using a stronger material. In-house made composite proved to be the weakest with the achieved diving depth of 15.5 m, while higher strength and carbon based composite hull model achieved 60 and 115 m diving depth prior to rupture, respectively.

The problem of stress concentration is pointed out, particularly for the main frame critical details and upper and lower hull parts joint at the submersible edges. Due to technological reasons, additional material may be present along the edge preserving therefore some stiffness which shell elements didn't take into account.

The article presents the procedure for the analysis of complex shape structures made of composite material. Such approach is best suited for the comparative analysis with cost-over-effort balance in mind. Additional material models and solid element modeling may be examined in the further research. Ideally, production version of hull should be tested and NFEM analysis verified and further calibrated.

REFERENCES

- [1] Armanios EA. Composite Materials Fatigue and Fracture. West Conshohocken: American Society for Testing and Materials, 1997.
- [2] Abot JL, Yasmin A, Daniel IM. Hygroscopic Behaviour of Woven Fabric Carbon – Epoxy Composites. *Journal of Reinforced Plastics and Composites* 2005;24(2):195-206.
- [3] Murphy J. Reinforced Plastics Handbook. Oxford, UK: Elsevier Science Ltd., 1998.
- [4] <http://www.dynasupport.com/howtos/material/composite-models>.
- [5] Heimbs S. Virtual testing of sandwich core structures using dynamic finite element simulations. *Computational Materials Science* 2009;45:205-216.
- [6] Kang KT et. al. Design of a composite roll bar for the improvement of bus rollover crashworthiness. *Composites: Part B* 2012;43:1705-1713.
- [7] Liu Q et. al. Lightweight design of carbon twill weave fabric composite body structure. *Composite Structures* 2013;97:231-238.
- [8] Hallquist JO. LS-DYNA Theoretical manual. Livermore: Livermore Software Technology Corporation, 1998.
- [9] Feraboli P, Wade B. Simulating Laminated Composites Using LS-DYNA Material Model MAT54 Part:I [0] and [90] Ply Single-Element Investigation. Baltimore: FAA JAMS, 2012.
- [10] LS-DYNA Keyword User's manual. Livermore: Livermore Software Technology Corporation, 2007.
- [11] Schweizerhof K, Weimar K, Munz T, Rottner T. Crashworthiness Analysis with Enhanced Composite Material Models in LS-DYNA – Merits and Limits. Karlsruhe: University of Karlsruhe, 1998.
- [12] Hyer MW. Stress Analysis of Fiber-Reinforced Composite Materials. Lancaster: DEStech Publications Inc., 1998.
- [13] Trifunović N. Autonomous Underwater Vehicle Bubblebee II. Zagreb: Faculty of Electrical Engineering and Computing, 2011 (in Croatian).

Submitted: 11.02.2014

Smiljko Rudan, Luka Drobilo

Accepted: 04.07.2014

University of Zagreb, Faculty of Mechanical Engineering and
Naval Architecture, Ivana Lučića 5, 10000 Zagreb, Croatia
srudan@fsb.hr